ISSN 1070-3632, Russian Journal of General Chemistry, 2017, Vol. 87, No. 12, pp. 3043–3051. © Pleiades Publishing, Ltd., 2017.

Synthesis of Nano-Metric Gold Complexes with New Schiff Bases Derived from 4-Aminoantipyrene, Their Structures and Anticancer Activity[1]

K. S. A. Abou Melha[a]*, G. A. A. Al-Hazmi[b,c], and M. S. Refat[d,e]

[a] *Chemistry Department, Faculty of Science of Girls, Abha, King Khalid University, Abha, Saudi Arabia*
**e-mail: dr.khlood@hotmail.com*

[b] *Chemistry Department, Faculty of Science, King Khalid University, Abha, Saudi Arabia*

[c] *Chemistry Department, Faculty of Applied Sciences, Taiz University, Taiz, Yemen*

[d] *Chemistry Department, Faculty of Science, Taif University, P.O. Box 888, Al-Hawiah, Taif, 21974 Saudi Arabia*

[e] *Department of Chemistry, Faculty of Science, Port Said, Port Said University, Egypt*

Received October 19, 2017

Abstract—Two new Schiff bases derived from combination of 4-aminoantipyrine with ethylenediamine (L_1) or benzaldehyde (L_2), gave Au(III) complexes. Their structures were elucidated from microanalytical, magnetic, conductance, and FT-IR, UV-Vis, Mass, and ^{1}H and ^{13}C NMR spectral data. High conductance values indicated electrolytic nature of the complexes. Magnetic moments and electronic spectral data indicated that two synthesized Au(III) Schiff base complexes had a square planar geometry. FT-IR spectroscopic data demonstrated that the Schiff bases were coordinated to Au(III) ions in a tetradentate manner with NNNN donor sites of two 4-amino antipyrine and two azomethine (L_1), while L_2 Schiff base ligand coordinated to Au(III) ions via its four azomethine nitrogen, which was further supported by the appearance of new bands in IR spectra due to ν(M–N). Activation thermodynamic parameters (E*, ΔH*, ΔS*, and ΔG*) were calculated on the basis of TG curves. Crystalline structures of Schiff bases and their Au(III) complexes were characterized by X-ray diffraction (XRD), their morphology was characterized by scanning electron microscopy (SEM) and transmission electron microscopy (TEM). The Schiff base ligands and their Au(III) chelates were screened for their antimicrobial activity. Cytotoxic activity of those was tested against the human breast cancer (MCF-7) and human hepatocellular carcinoma (HepG-2) tumor cell lines.

Keywords: 4-aminoantipyrine, gold, Schiff base, chelates, nanoscale, spectroscopic, morphology, antimicrobial activity

DOI: 10.1134/S1070363217120519

INTRODUCTION

Transition metal complexes of 4-aminoantipyrine and its derivatives have been extensively studied due to their potential in biology [1].

The literature survey reveals that close attention has been payed to Schiff bases derived from 4-amino-antipyrine with several aldehydes or ketones. Less efforts were directed towards condensation of 4-amino-antipyrine with ethylenediamine in the presence of benzaldehyde condensed with the NH_2 group in the position 4. In the present study two new tetradentate Schiff bases and their Au(III) complexes were synthesized and characterized by elemental, molar conductance, magnetic, SEM, TEM, and thermal analyses, and a variety of spectral methods including Mass, UV-Vis, FT-IR, ^{1}H and ^{13}C NMR spectrum, and XRD. The results of their antibacterial and anticancer activity tests are reported herein.

EXPERIMENTAL

4-Aminoantipyrine (Aldrich), ethylenediamine (Sigma-Aldrich), benzaldehyde (Aldrich), gold(III) chloride (Sigma-Aldrich), and all other chemicals and solvents were of analytical grade and used without further purifications.

The elemental analyses were carried out on a Perkin Elmer CHN 2400 (USA). Molar conductivity of

[1] The text was submitted by the authors in English.

Scheme 1.

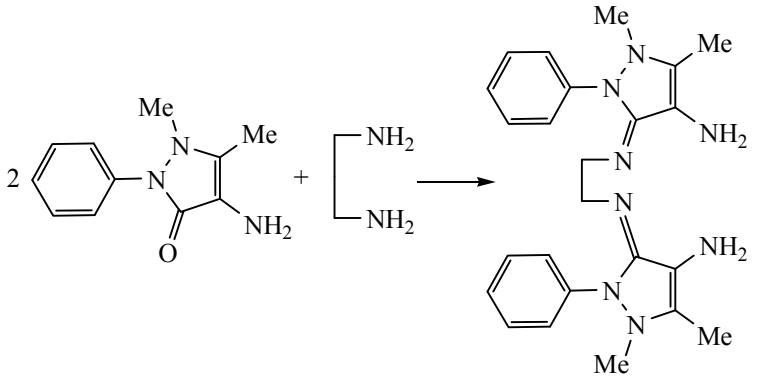

Scheme 2.

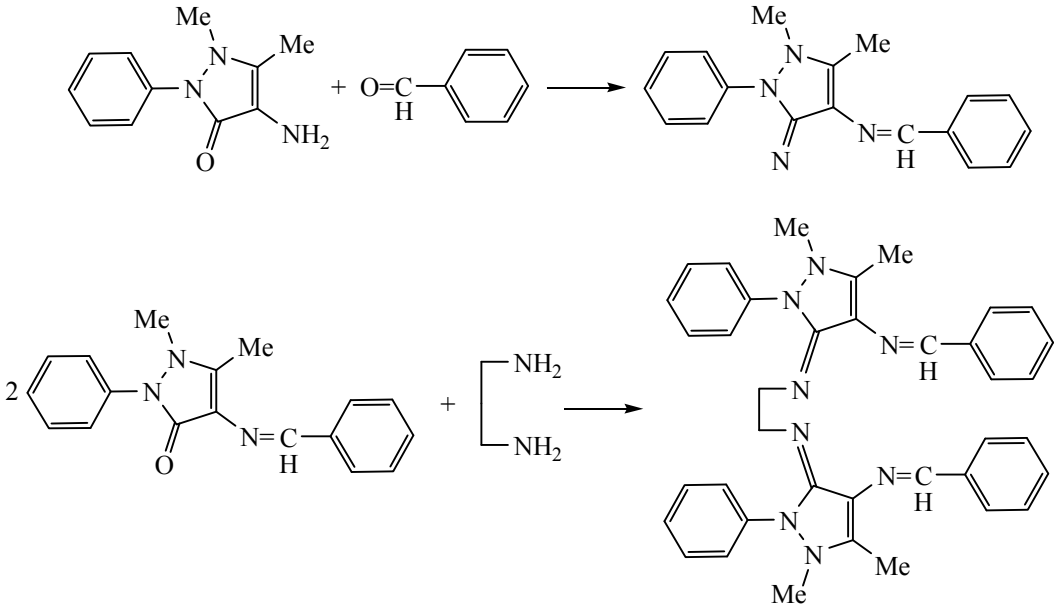

freshly prepared 1.0×10^{-3} mol/cm^3 DMSO solutions was measured using a Jenway 4010 conductivity meter. IR spectra were recorded on a Bruker FT-IR Spectrophotometer (4000–400 cm^{-1}). UV-Vis absorption spectra were recorded in DMSO in the range of 800–200 nm on a UV2 Unicam UV/Vis Spectrophotometer fitted with a quartz cell of 1.0 cm path length. Magnetic moments were measured on a Magnetic Susceptibility Balance, Sherwood Scientific, Cambridge Science Park, England, at 25°C. ^{1}H and ^{13}C NMR spectra were measured on a Varian Mercury VX-300 NMR spectrometer in DMSO-d_6. Chemical shifts were related to those of the solvent. Purity of Schiff base ligands (L_1 and L_2) was tested by mass spectra measured on a AEI MS 30 Mass Spectrometer. The thermal studies, TG/DTG–50H, were carried out on a Shimadzu thermo-gravimetric analyzer under nitrogen up to 800°C. Scanning electron microscopy (SEM) images were taken with a Quanta FEG 250 equipment. The X-ray diffraction patterns were recorded on an X'Pert PRO PANanalytical X-ray powder diffractometer. Transmission electron microscopy images (TEM) were generated using a JEOL 100s microscope.

Synthesis of 4-aminoantipyrine ethylenediamine Schiff base chelate (L_1) (Scheme 1). 4-Aminoantipyrine (2.03 g, 0.02 mol, 20 mL methanol) was mixed with ethylenediamine (0.6 g, 0.01 mol, 20 mL methanol) and refluxed for 2 h at 60°C. The precipitate was washed, filtered off, recrystallized from methanol, and dried in a vacuum desiccator over anhydrous calcium chloride. The product was obtained as a yellow solid, yield 61%, mp 220°C. ^{1}H NMR spectrum, δ, ppm: 1.77 s (6H, 2CH_3, C^3); 2.1 s (4H, 2CH_2);

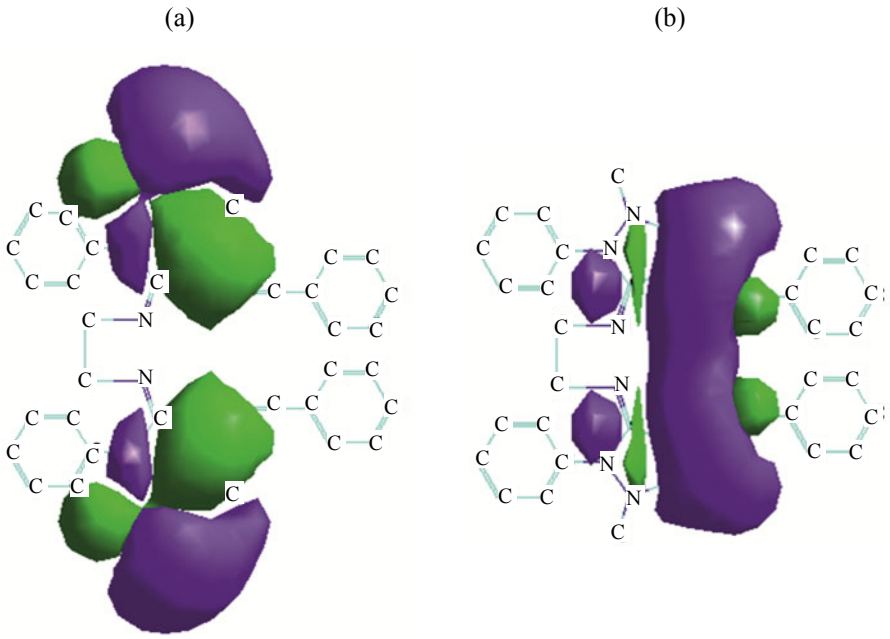

Fig. 1. (a) HOMO and (b) LUMO structures of Schiff base ligand L_2.

2.74 s (6H, $2NCH_3$); 3.99 br (4H, $2NH_2$); 7.21 t (2H, phenyl, C^4); 7.40 m (8H, phenyl, C^2, C^3). ^{13}C NMR spectrum, δ, ppm: 10.35, 23.76 ($2CH_3$), 38.73 (CH_2), 120.5, 122.3, 125.6, 129.6, 136.0, 161.8, 169.8, 174.2 (N–C, C=C, C=N). MS, *m/z* (I_{rel}, %), $[M]^+$: 430 (4.7), 401 (2.5), 243 (2.7), 216 (41.3), 201 (31.7), 186 (22.5), 185 (52.1), 134.8 (48.6), 124 (22.8), 109 (22.4), 105 (36.4), 78 (100), 57 (80). Found, %: C 66.80; H 6.87; N 25.79. $C_{24}H_{30}N_8$. Calculated, %: C 66.95; H 7.02; N 26.03.

Synthesis of 4-aminoantipyrine–benzaldehyde–ethylenediamine Schiff base chelate (L_2) (Scheme 2). The Schiff base chelate (L_2) was synthesized in two steps. Solution of 4-aminoantipyrine (2 mmol) in methanol was mixed with benzaldehyde (2 mmol) and gently heated for 2 h upon constant stirring. The precipitate obtained was filtered off and recrystallized from methanol. Fine pale yellow powder was washed with alcohol, ether and dried in *vacuum* desiccator over anhydrous calcium chloride. The precursor (2 mmol) was mixed with methanol solution of ethylenediamine (1 mmol) and refluxed for 2 h with constant stirring at 60°C. The reaction mixture was poured in to crushed ice. The yellow solid product (L_2) was filtered off and recrystallized from methanol. Yield 63%, mp 209°C. ^1H NMR spectrum, δ, ppm: 2.18 s (6H, $2CH_3$, C^3); 2.69 s (4H, $2CH_2$); 3.11 s (6H, $2NCH_3$); 7.35–7.83 m (20H, phenyl). ^{13}C NMR spectrum, δ, ppm: 12.59, 34.83 ($2CH_3$), 52.16 (CH_2), 122.7, 123.3, 126.8, 127.2, 130.3, 132.2, 133.6, 133.8, 135.9, 146.4, 158.0, 162.5 (N–C, C=C, C=N). MS, *m/z* (I_{rel}, %), $[M]^+$: 606 (14.4), 591 (12.3), 503 (10.5), 318 (43.9), 290 (35.7), 289 (25.4, 213 (24.5), 198 (22.7), 187 (48.9), 186 (28.8), 172 (30.2), 105 (15.3), 104 (11.2), 95 (54.4), 77 (100). Found, %: C 75.09; H 6.22; N 18.41. $C_{38}H_{30}N_8$. Calculated, %: C 75.22; H 6.31; N 18.47.

Synthesis of Au(III) Schiff base (L_1–L_2) complexes. The mixture of a Schiff base ligand (L_1 or L_2) (0.02 mol) with gold(III) chloride (0.02 mol) was dissolved in 50 mL methanol and refluxed for 2 h. Then, the red (L_1) or brown (L_2) solution was evaporated to half of its original volume to make the product precipitate. The precipitate was filtered off, washed with methanol and dried in a *vacuum* desiccator over anhydrous $CaCl_2$.

$[Au(L_1)]\cdot Cl_3$. Yield 60%, decomposition temperature 260–280°C. ^1H NMR spectrum, δ, ppm: 1.90 s (6H, $2CH_3$, C^3); 2.5 s (4H, $2CH_2$); 2.84 s (6H, $2NCH_3$); 4.81 br (4H, $2NH_2$); 7.38–7.59 m (10H, phenyl). ^{13}C NMR spectrum, δ, ppm: 15.73, 27.08 ($2CH_3$), 45.95 (CH_2), 122.5, 123.5, 126.6, 129.0, 137.5, 160.6, 170.5, 179.8 (N–C, C=C, C=N). MS, *m/z* (I_{rel}, %): 376 (26.9), 375 (55.7), 361 (24.5), 204 (46.7), 203 (73.9), 202 (28.8), 120 (17.4), 93 (74.4), 84 (31.2), 83 (38.5), 76 (58.1), 56 (100). Found, %: C 39.10; H 4.03; N 15.14; Cl 14.33. Calculated, %: C 39.28; H 4.12; N 15.27; Cl 14.49.

Scheme 3. The proposed structures of $[Au(L_1)]\cdot Cl_3$ and $[Au(L_2)]\cdot Cl_3$ complexes.

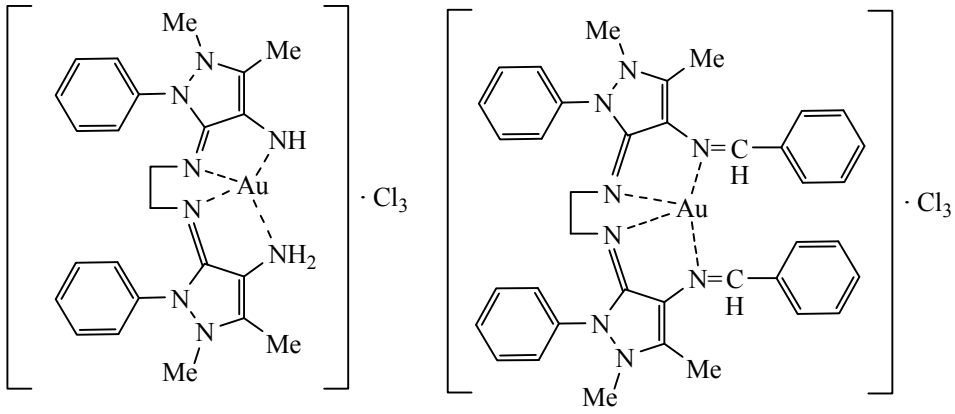

$[Au(L_2)]\cdot Cl_3$. Yield 64%, decomposition temperature 260–274°C. Found, %: C 49.89; H 4.12; N 12.08; Cl 11.48. Calculated, %: C 50.15; H 4.21; N 12.31; Cl 11.69.

Antimicrobial assessment. Antimicrobial activity of the samples was tested using the modified Kirby-Bauer disc diffusion method [2]. Briefly, 100 μL of the best bacteria (gram negative (*Escherichia coli* and *Klebsiella*) and gram positive (*Staphylococcus aureus* and *Staphylococcus epidermidis*) were grown in 10 mL of fresh media until they reached a count of approximately 108 cells/mL for bacteria [3]. Microbial suspension (100 μL) was spread onto agar plates, corresponding to the broth in which they were maintained. Isolated colonies of each organism were selected from primary agar plates and tested for susceptibility by the disc diffusion method [4].

Anti-cancer activity. Human breast cancer (MCF-7) cell line and human hepatocellular carcinoma (HepG-2) cells were obtained from the American type culture collection ATCC, Rockvill, MD). The cells were grown on RPMI-1640 medium supplemented with 10% inactivated fetal calf serum and 50 μg/mL of gentamycin. The cells were maintained at 37°C in a humidified atmosphere with 5% CO_2 and were subcultured two to three times a week. The cells were grown as monolayers in growth RPMI-1640 medium supplemented with 10% inactivated fetal calf serum and 50 μg/mL of gentamycin. The monolayers of 10000 cells adhered at the bottom of the wells in a 96-well micro titer plate were incubated for 24 h at 37°C in a humidified incubator (5% CO_2). The monolayers were then washed with sterile phosphate buffered saline (0.01 M pH 7.2) and simultaneously the cells were treated with 100 μL of the test sample different

Table 1. Quantum chemical parameters of the Schiff base ligands L_1 and L_2

Parameter	L_1	L_2
E_{LUMO}, eV	–23.5691	–29.4767
E_{HOMO}, eV	4.2669	22.62484
ΔE, kJ/mol	27.836	52.10154
χ, kJ/mol	9.6511	3.42593
η, kJ/mol	13.918	26.05077
σ, kJ/mol	0.071849	0.038387
P_i, kJ/mol	–9.6511	–3.42593
S, kJ/mol	0.035925	0.019193
ω, kJ/mol	3.346161	0.225272
ΔN_{max}, kJ/mol	0.693426	0.13151

Table 2. FT-IR spectral data (cm^{-1}) for L_1, L_2 and their gold(III) complexes

Compounds	ν(N–H); ν(NH_2)	ν(C=O)	ν(C=N)	ν(C–N)	ν(M–N)
L_1	3436, 3322	1649	1649, 1585	1274	–
$[Au(L_1)]Cl_3$	3423, 3135	–	1636	–	499
L_2	–	–	1649, 1561	1298	
$[Au(L_2)]Cl_3$			1623, 1511	1286	499

Table 3. Kinetic parameters deduced from the Coats–Redfern equation for the gold(III) complexes

Complexe	DTG_{max}, °C	Steps	Thermodynamic parameters	
			parameter	value
$[Au(L_1)]\cdot Cl_3$	277		E, J/mol	4.49×10^4
			A, s^{-1}	4.61×10^1
		2	ΔS, J mol^{-1} K^{-1}	-2.18×10^2
			ΔH, J/mol	4.02×10^4
			ΔG, J/mol	1.64×10^5
			r	0.9995
$[Au(L_2)]\cdot Cl_3$	300		E, J/mol	6.25×10^4
			A, s^{-1}	6.60×10^3
		2	ΔS, J mol^{-1} K^{-1}	-1.77×10^2
			ΔH, J/mol	5.80×10^4
			ΔG, J/mol	1.52×10^5
			r	0.9950

dilutions in fresh medium and incubated at 37°C. Control of untreated cells was made in the absence of the test sample. Six wells were used for each concentration of the test sample. Every 24 h observations under an inverted microscope were made. Number of the surviving cells was determined by staining the cells with crystal violet [5] followed by cell lysing using 33% glacial acetic acid and the absorbance was determined at 490 nm using an ELISA reader (Sun Rise, TECAN, Inc, USA) after intensive mixing. The absorbance values from untreated cells were considered as 100% proliferation. The number of viable cells was determined using an ELISA reader as mentioned before and the percent of viability was calculated as

$$[1 - (OD_t/OD_c)]\times100\%,$$

where OD_t is the mean optical density of wells treated with the test sample and OD_c is the mean optical density of untreated cells. The 50% inhibitory concentration (IC_{50}) was estimated from graphic plots.

RESULTS AND DISCUSSION

Molecular modeling. The Schiff base chelates and their gold(III) complexes single crystals data were supported by quantum chemical calculations and molecular modeling studies [6,7]. The geometry optimization and conformation analysis were performed using semi-empirical PM3 level [7] as implemented in software of Hyperchem 7.5 program [8] (Table 1).

The negative data of E_{LUMO} and E_{HOMO} indicated stability of the synthesized complexes. High values of E_{HOMO} confirmed that the Schiff base ligands had a powerful donation character. Molecular modeling allowed to estimate three dimensional arrangements of atoms in free Schiff base and their Au(III) complexes. As an example, structures of HOMO and LUMO for the Schiff base ligand L_2 are presented in Fig. 1.

Stoichiometry and molar conductance results. Two tetradentate Schiff base ligands and their gold(III) complexes have been synthesized by a 1 : 1 molar condensation of 4-aminoantipyrine with ethylenediamine or benzaldehyde. The complexes were stable in the air at room temperature, slightly soluble in polar solvents and soluble in organic solvents (DMF, DMSO). Molar conductances of the complexes were 59 and 72 μs/cm for gold(III) complexes of L_1 and L_2, respectively. These results indicated that gold(III) complexes were 1 : 1 electrolytes in DMSO solutions (1×10^{-3} M). The electrolytic nature of Au(III) complexes suggested that the chloride anions of the salts were localized outside the coordination spheres [9] (Scheme 3). This was supported by the reaction of the synthesized gold(III).

IR spectra. IR spectra of the ligands as well as those of Au(III) complexes had similar profiles (Table 2). Condensation of 4-aminoantipyrine with ethylenediamine was indicated by disappearance of the band ν (C=O), presence of the NH_2 group stretching bands [10] and a band at 1585 cm^{-1} assigned to the ν(C=N) group (Table 2). The band at 1649–1585 cm^{-1} (C=N) of the ligand L_1 disappeared or shifted to lower frequencies (1636 cm^{-1}) in the spectrum of the corresponding gold(III) complex, which indicated participation of C=N nitrogen in coordination with

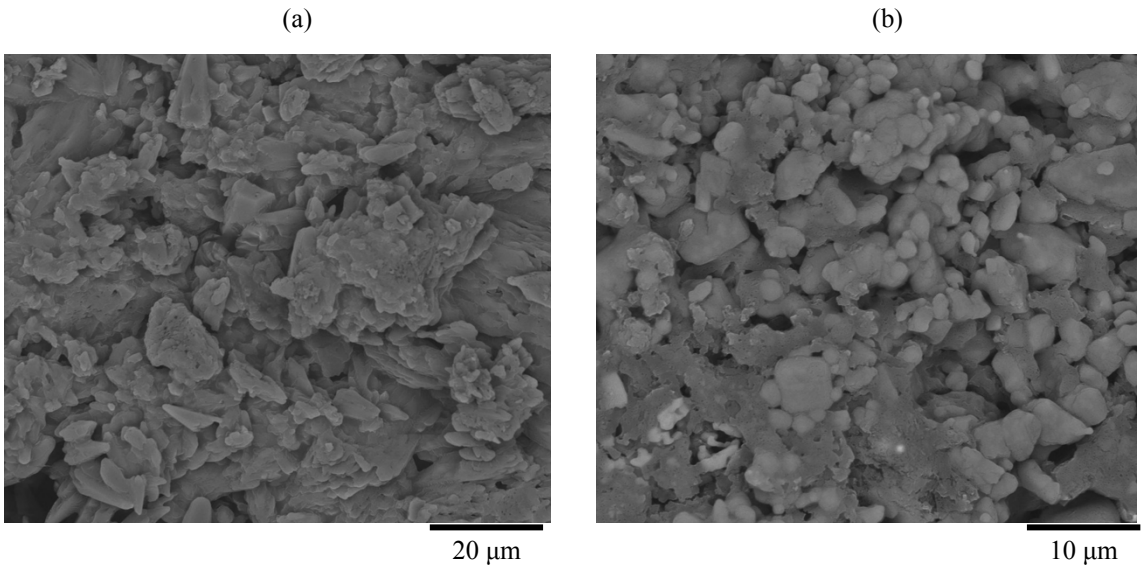

Fig. 2. SEM images of Schiff base ligand (a) L_1 and (b) $[Au(L_1)]\cdot Cl_3$ complex.

Au(III). Stretching vibrations of the NH_2 group were shifted to lower wavenumbers in the spectra of the complex due to participation of nitrogen atoms of the terminal amino groups in chelation. The ligand acted as tetradentate chelating agents bonded to gold(III) ion via four nitrogen atoms of the Schiff base (C=N and NH_2). Appearance of the weak band at 499 cm^{-1} confirmed the M···N coordination in the complex.

Electronic and magnetic measurements. Au(III) Complexes of L_1 and L_2 Schiff bases had diamagnetic nature (μ_{eff} = 0.21 and 0.19) as expected for low spin d^8 complexes, which was assigned to square planar geometry [11].

Electronic spectra of free Schiff base ligands exhibited bands at 292 and 352 nm, assignable to π–π* and *n*–π* transitions in the benzene rings, NH_2 and azomethine groups. The electronic spectra of gold(III) complexes gave three distinguished absorption bands at 383–379, 354, and 292–280 nm due to $^1A_{1g}\rightarrow{}^1A_{2g}$, $^1A_{1g}\rightarrow{}^1B_{1g}$, $^1A_{1g}\rightarrow{}^1E_g$ and charge transfer transitions, respectively. The bands were attributed to the low-spin square planar configuration [12].

^{1}H and ^{13}C NMR spectra. Two methyl groups signals of the free L_1 recorded in ^{1}H NMR spectrum (1.77 and 2.74 ppm) shifted in the spectrum of the corresponding complex to 1.90 and 2.84 ppm accordingly. The signals of the NH_2 group shifted from 3.99 to 4.81 ppm, accordingly, indicating lower electronic density over the nitrogen atom upon complexation. The ^{13}C NMR spectrum demonstrated clear downfield shift for the sp^3 carbon atoms.

Table 4. Crystallite sizes (*D*), dislocation density (δ) and strain (ε) data for $[Au(L_1)]Cl_3$

Complex	*D*, nm	$\delta\times10^{12}$, lin/m^2	$\varepsilon\times10^{-4}$
$[Au(L_1)]\cdot Cl_3$	12	0.0069	1.65

Thermogravimetric analyses and kinetic calculations. Decomposition temperature of the synthesized gold(III) complexes was above 200°C which indicated formation of stable coordination compounds.

In the current study, the integral method of Coats and Redfern [13] was used to evaluate the kinetic parameters and thermal behavior of gold(III) Schiff base complexes (Table 3). The accumulated data allowed to make the following remarks:

(1) The gold(III) Schiff base complexes demonstrated the first order decomposition stages in all cases.

(2) The value of ΔG increased significantly for the subsequent decomposition stages of a given complex. This was due to increased values of $T\Delta S$ from one stage to another that were higher than the values of ΔH [14, 15].

(3) The negative values of activation entropy (ΔS) indicated the more ordered activation complexes than the reactants and/ or the reactions were slow [16].

(4) The positive values of ΔH indicated that the decomposition processes were endothermic.

Table 5. Inhibition zone diameter for Schiff bases and their gold(III) complexes against some kinds of bacteria

Samples		Inhibition zone diameter, mm/mg sample			
		Klebsiella (g_-)	*Escherichia coli* (g_-)	*Staphylococcus Epidermidis* (g_+)	*Staphylococcus Aureus* (g_+)
Control: DMSO		0.0	0.0	0.0	0.0
Standards	Augmentin	0.5	0.3	1.0	0.4
	Unasyn	0.2	0.1	1.0	0.2
L_1		0.3	0.1	0.0	0.0
Au–L_1 complex		0.2	0.2	0.0	0.0
L_2		0.2	0.0	0.0	0.0
Au–L_2 complex		0.1	0.0	0.0	0.0

Morphological studies (XRD, SEM and TEM). Crystallinity of the Schiff base chelate (L_1) and its Au(III) complex were deduced from the major diffraction patterns based on the Deby–Scherrer [17]:

$$D = K\lambda/\beta\cos\theta,$$

where λ is the wavelength of X-ray (1.5418 Å) for CuK_α radiation, K is constant taken as 0.94, β full width at half maximum (FWHM) of prominent intensity peak (100% relative intensity peak), θ is a peak position.) The calculated grain sizes were found to be 12 nm for $[Au(L_1)]\cdot Cl_3$ complex. The lower grain size of Au(III)–L_1 complex (12 nm) could be attributed to the increase of Schiff base chelates around metal ions as tetradentate cavity [18]. The evaluated dislocation density (δ) [19] and is listed in Table 4.

Four diffraction patterns peaks at 2θ = 38.14°, 44.30°, 64.59°, and 77.63°, were assigned to the planes (111), (200), (220), and (311) of face centered cubic crystal lattice structure of AuNPs [20]. The average particle size was found to be 12 nm, which corresponded to the planes (111), (200), (220), and (311) deduced from the Scherrer's equation [21, 22].

According to the SEM images (Fig. 2) the synthesized gold(III) complex was NPs, grown as uniform shape with diameter size range 0.3–3.0 μm.

The TEM analysis of the complex $[Au(L_1)]\cdot Cl_3$ (Fig. 3) confirmed the presence of nanomeric gold(III) ions inclusion in Schiff base molecules. The TEM photograph demonstrated spherical NPs of gold(III) that appeared as dark spots. The diameter of Au(III) complex was ca 10 nm. These data matched with the XRD data.

Antibacterial and anticancer assessments. Antibacterial activity of the Schiff base ligands (L_1 and L_2) and their gold(III) complexes was screened *in vitro* against gram negative (*Escherichia coli* and *Klebsiella*) and gram positive (*Staphylococcus aureus* and *Staphylococcus epidermidis*) bacteria (Table 5). The accumulated data indicated that the gold(III) complexes exhibited higher growth inhibition potential than that of the ligand. The $[Au(L_1)]\cdot Cl_3$ complex demonstrated antibacterial activity against *Escherichia coli* that inhibited multiplication process of the microbes by blocking their active sites. Mechanism of higher toxicity of the gold(III)–L_1 complex compared to that of the L_1 ligand could be ascribed to the increase of lipophilicity of the complex due to chelation [23]. Chelation reduced polarity of the metal atom mostly due to partial sharing of its positive

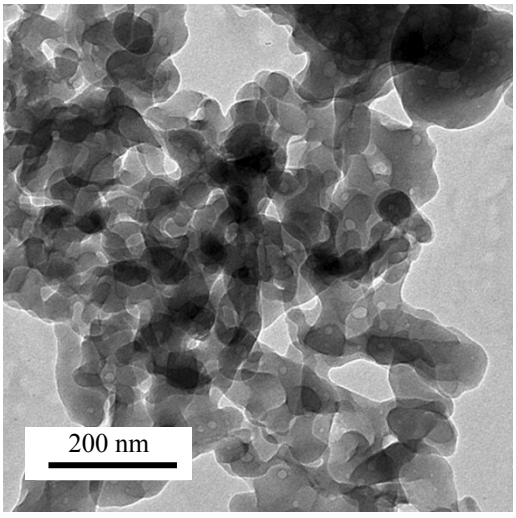

Fig. 3. TEM image of $[Au(L_1)]\cdot Cl_3$ complex.

Table 6. Inhibitory activity of the Schiff base ligand L_1 and complexes $[Au(L_1)]\cdot Cl_3$ and $[Au(L_2)]\cdot Cl_3$ against MCF-7 and HepG-2 cell lines

Sample concentration, μg	Viability					
	HepG-2 cell line			MCF-7 cell line		
	L_1	Au–L_1	Au–L_2	L_1	Au–L_1	Au–L_2
500	11.78	6.39	8.62	24.47	8.94	12.45
250	24.02	16.47	19.73	37.56	17.25	24.56
125	32.76	28.92	28.65	59.21	28.19	39.72
62.5	46.28	37.54	39.51	80.46	37.85	58.19
31.25	71.39	45.23	48.62	95.28	60.94	79.04
15.60	86.23	68.96	70.38	99.72	78.15	94.18
7.80	94.12	82.37	86.29	100	92.47	99.72
3.90	99.47	90.49	97.02	100	98.42	100
2	100	97.51	100	100	100	100
1	100	100	100	100	100	100
0	100	100	100	100	100	100
IC_{50}	57.9	28.1	30.2	178	46.1	90.2

charge with the donor groups and possible π-electron delocalization within the whole chelate ring. Chelation could also increase lipophilic nature of the central metal atom, which subsequently favored permeation through the lipid layer of cells membrane [24]. The mode of action of complexes could involve formation of hydrogen bonds with the imino group leading to interference with the cell wall synthesis. H-Bond formation would have damaged the cytoplasmic membrane and the cell permeability could also be altered leading to cells death.

In vitro cytotoxicity assessment of the free Schiff base (L_1) and gold(III) complexes were operated on human breast cancer (MCF-7) cell line and human hepatocellular carcinoma (HepG-2) tumor cell lines in the presence of the standard drug. The results were evaluated upon determination of inhibitory concentration of 50% (IC_{50}) (Table 6). According to the presented data, gold(III) complexes were more efficient against HepG-2 cell line than MCF-7 cell line.

ACKNOWLEDGMENTS

This work was supported by grants from Deanship of Scientific Research, King Khalid University, Saudi Arabia under project grants nos. 38-224-G.R.P.

REFERENCES

1. Agarwal, R.K., Sharma, D., Singh, L., and Agarwal, H., *Bioinorg. Chem. Appl.,* 2006, vol. 2006, p. 1. doi 10.1155/BCA/2006/29234
2. Bauer, A.W., Kirby, W.A., Sherris, C., and Turck, M., *Am. J. Clin. Pathology*, 1966, vol. 45, p. 493.
3. Pfaller, M.A., Burmeister, L., Bartlett, M.A., and Rinaldi, M.G., *J. Clin. Microbiol*., 1988, vol. 26, p. 1437.
4. *National Committee for Clinical Laboratory Standards, Performance Volume. Antimicrobial Ausceptibility of Flavobacteria*, 1997.
5. Mosmann, T., *J. Immunol. Methods*, 1983, vol. 55, p. 65. doi 10.1016/ 0022-1759(83)90303-4
6. Yousef, T.A., Abu El-Reash, G.M., and El Morshedy, R.M., *J. Mol. Struct*., 2013, vol. 1045, p. 145. doi 10.1016/ j.molstruc.2013.03.060
7. Helal, M.H., El-Awdan, S.A., Salem, M.A., Abd-elaziz, T.A., Moahamed, Y.A., El-Sherif, A.A., and Mohamed, G.A.M., *Spectrochim. Acta, Part A*, 2015, vol. 135, p. 764. doi 10.1016/j.saa.2014.06.145.
8. *Hyper Chem*, Version 7.51 Hyper cube, INC.
9. Refat, M.S., *J. Mol. Struct*., 2007, vol. 842, p. 24. doi 10.1016/j.molstruc. 2006.12.006.
10. Nakamoto, K., *Infrared and Raman Spectra of Inorganic and Coordination Compounds*, New York: Wiely, 1978.

11. Abdalrazaq, E.A., Buttrus, N.H., and Abd Al-Rahman, A.A., *Asian J. Chem.*, 2010, vol. 22, p. 2179.
12. Tunney, J.M., Blake, A.J., Davies, E.S., Mcmater, J., Wilson, C., and Garner, C.D., *Polyhedron*, 2006, vol. 25, p. 591. doi 10.1016/j.poly.2005.09.002
13. Coats, A.W. and Redfern, J.P., *Nature*, 1964, vol. 201, p. 68. doi 10.1038 /201068a0
14. Maravalli, P.B. and Goudar, T.R., *Thermochim Acta* 1999, vol. 325, p. 35. doi 10.1016/S0040-6031(98) 00548-6
15. Yusuff, K.K.M. and Sreekala, R., *Thermochim Acta* 1990, vol. 159, p. 357. doi 10.1016/0040-6031(90) 80121-E.
16. Frost, A.A. and Peasron, R.G., *Kinetics and Mechanism*, New York: Wiley, 1961.
17. Cullity, B.D., *Elements of X-ray Diffraction*, Addison-Wesley, Reading, MA, 1972, p. 102.
18. Salavati-Niasari, M., Mohandes, F., Davar, F., Mazaheri, M., Monemzadeh, M., and Yavarinia, N., *Inorg. Chim. Acta* 2009, vol. 362, p. 3691. doi 10.1016/ j.ica.2009.04.025.
19. Velumani, S., Mathew, X., and Sebastian, P.J., *Solar Energy Mater. Solar Cells*, 2003, vol. 76, p. 359. doi 10.1016/S0927-0248(02)00288-X
20. Zhang, Y., Wei, S., and Chen, S., *Int. J. Electrochem. Sci*., 2013, vol. 8, p. 6493.
21. Shi, W., Casas, J., Venkataramasubramani, M., and Tang, L., *Int. Scholar. Res*. *Network ISRN Nanomater*., 2012, vol. 2012, p. 1. doi 10.5402/2012/ 659043.
22. Monshi, A., Foroughi, M.R., and Monshi, M.R. *World J. Nano. Sci. Engin*., 2012, vol. 2, p. 154. doi 10.4236/ wjnse.2012.23020
23. Haergreaves, M.K., Pritchard, J.G., and Dave, H.R., *Chem. Res*., 1970, vol. 70, p. 439. doi 10.1021/ cr60266a001.
24. Dharmaraj, N., Viswanathamurthi, P., and Natarajan, K., *Trans. Met. Chem*., 2001, vol. 26, p. 105. doi 10.1023/ A:100713240